From interface laws to composite behaviour

Sørensen, Bent F.; Mikkelsen, Lars Pilgaard; Østergaard, R.C.; Goutianos, Stergios

Published in:
Interface design of polymer matrix composites - mechanics, chemistry, modelling and manufacturing. Proceedings

Publication date:
2007

Document Version
Publisher's PDF, also known as Version of record

Proceedings of the 28th Risø International Symposium on Materials Science:
Interface Design of Polymer Matrix Composites – Mechanics, Chemistry, Modelling and Manufacturing
Editors: B. F. Sørensen, L. P. Mikkelsen, H. Lilholt, S. Goutianos, F. S. Abdul-Mahdi
Risø National Laboratory, Roskilde, Denmark, 2007

FROM INTERFACE LAWS TO COMPOSITE BEHAVIOUR

Bent F. Sørensen, Lars P. Mikkelsen, Rasmus C. Østergaard
and Stergios Goutianos

Materials Research Department, Risø National Laboratory,
Technical University of Denmark, Roskilde, Denmark

ABSTRACT

This paper summarizes efforts to characterize, model and link the mechanic response of polymer matrix composites from nanoscale, through microscale to macroscale. Particular attention is given to cracking parallel to the fibre direction. For this failure mode, large scale crack bridging occurs by cross-over bridging. Mechanical characterization is made in the form of interface cohesive laws, representing the fracture process zone of the fibre/matrix interface. Micromechanical models are use for prediction of composite cohesive laws, representing crack bridging for the cross-over bridging mechanism. Comparisons are made between model and experiments.

1. INTRODUCTION

Polymer matrix composites based on aligned, continuous fibres have gained widespread use in engineering applications, in particularly in load-carrying structures where weight savings are of high importance (Brøndsted et al. 2005). Furthermore, composite materials offer the possibility of tailor-making materials for specific purposes, since they can be designed at many scales. Typically, composites are considered from the nanometer scale, over the micrometer scale, lamina (or ply) level to laminate and macroscale. Although a number of models exist at the various scales, it is still fair to claim that a complete understanding of how macroscale properties of composite materials depend on micro- and nanometer scale parameters does not yet exist.

It is therefore a long term ambition in materials research is to create a comprehensive knowledge of the connection between the various scales, so that fibre composites can readily be designed at the nanometer scale for optimal macro scale properties, e.g. high tensile strength and high fracture toughness.

At the shorter term a goal is to focus at the effect of the fibre/matrix interface properties. Fig. 1 shows a schematic of how properties of the fibre/matrix interface at nanoscale can be connected

to the composite behavior at the microscale and macroscale. At the nanometer scale the interface can be described the fibre surface, which has characteristic roughness characteristics. The surface roughness and chemistry can be manipulated and it is anticipated that the roughness and chemistry at the fibre/matrix interface plays a key role in controlling the fracture behavior of the composite material.

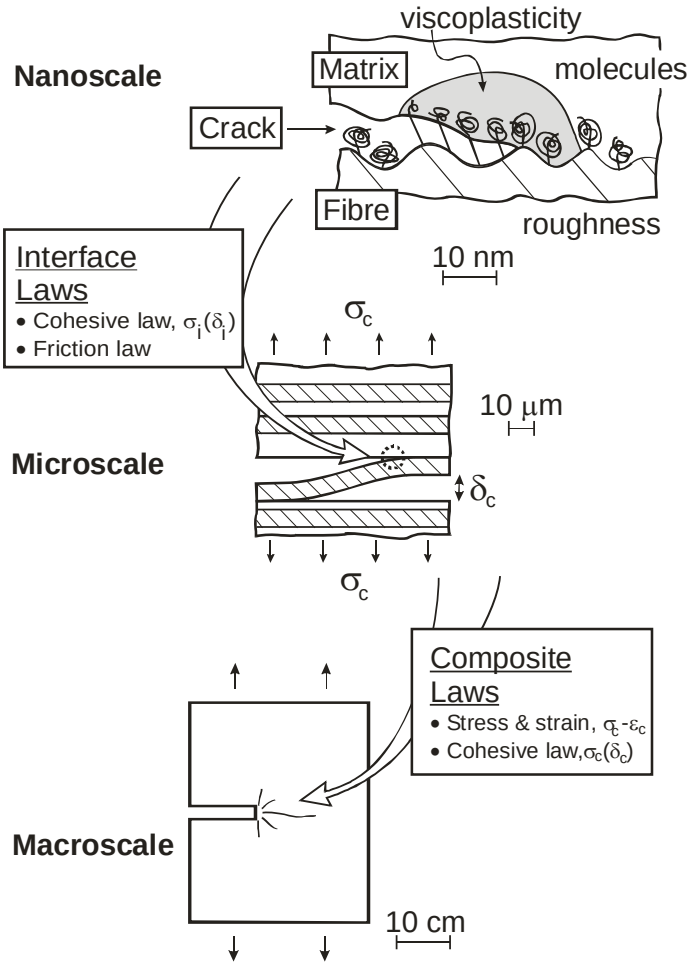

Fig. 1. The interface law represents the mechanical response of the interface (as controlled by chemistry and surface roughness) by connecting surfaces at the microscale. The composite law is used at macroscale to rep-resent the interaction between the discrete fibre, matrix and crack in a continuum model where the composite is treated as a homogenized anisotropic continuum.

One of the ways to modify the fibre/matrix interface is to graft long molecule chains to the surface so that the molecules are pulled out during interface separation. If the forces from the molecules are sufficiently high, they may result in the formation of a (visco-)plastic zone at the crack tip. This is expected to cause the fracture toughness of the interface to increase (Tvergaaard and Hutchinson, 1993). Thus, the nanoscale/microscale levels can only be understood by a combination of skills belonging to chemistry and to mechanics.

From the perspective of mechanics, one of the challenges is to characterize the interface behavior properly. Earlier, the mechanics of a fibre/matrix interface was characterized in terms of a maximum shear stress. Models and experiments such as the single fibre fragmentation test rely on determination of a critical shear strength for the interface. More recent models and test methods are based on fracture mechanics and incorporate interface fracture energy for fibre/matrix debonding. However, even this approach has it shortcomings. The most severe issue

concerns the interplay with plasticity in the matrix. The size of the crack tip fracture process zone and the surrounding plastic zone can be comparable or larger than the spacing between the fibres. Then fibre/matrix debonding becomes a so-called Large-Scale-Failure-Process problem, implying that it cannot be properly analyzed in terms of Linear Elastic Fracture Mechanics (LEFM).

We favor an approach where the interface separation is described in terms of a cohesive law. Cohesive laws have been used to represent failure from the microscale to the macroscale (Needleman 1987; Tvergaard and Hutchinson 1993; Mohammad and Liechti 2000; Yang and Thouless 2001; Yang and Cox 2005). We will denote the cohesive law of the fibre/matrix interface by *interface cohesive law*. The use of a representation based on interface cohesive laws allows the separation of fracture energy due to the decohesion process and the energy dissipation due to crack tip plasticity.

In the present paper, we focus at the development of methods that allow the determination of interface cohesive laws. Having obtained interface cohesive laws, they can be used for prediction cohesive laws at the macroscale. In the present paper we will call cohesive laws at the macroscale for *composite cohesive laws*. We illustrate interface cohesive laws and composite cohesive laws in Fig. 1. The principle of modeling a fracture process zone by a cohesive zone is shown schematically in Fig. 2.

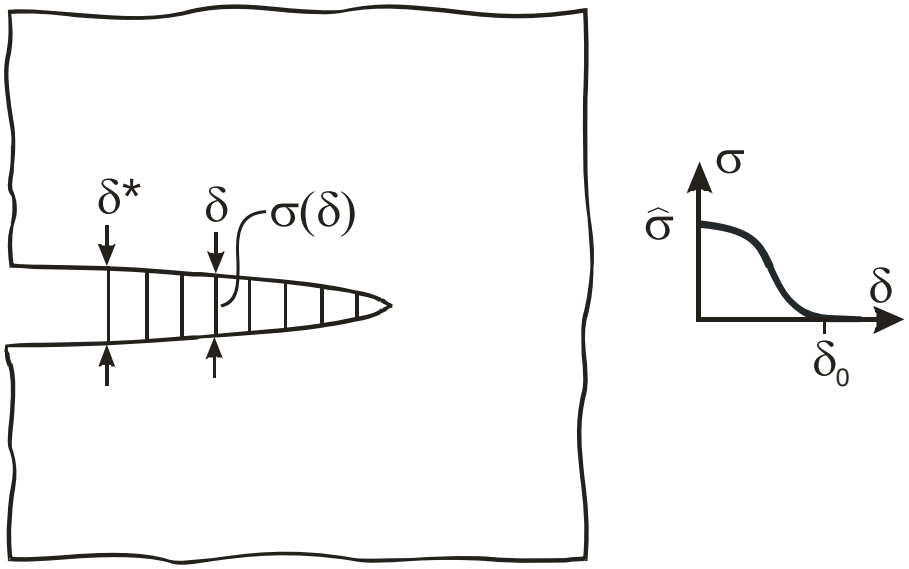

Fig. 2. A fracture process zone can be modeled by a cohesive zone. The cohesive law is the relationship between opening and the stress transmitted across the fracture process zone. The area under the curve represents the fracture energy.

The major macroscale problem that we address in the present paper is cracking along a weak plane parallel to the fibre direction, e.g. delamination (interlaminar cracking) and splitting (intralaminar cracking). This cracking mode can be accompanied by large scale fibre bridging, which from a safety point of view is beneficial since it leads to rising fracture resistance (R-curve behavior). Obviously, the fracture resistance increase depends on the fibre/matrix interface properties. It is therefore of interest to establish tools that can characterize and model fibre bridging in composite materials at various scales.

The paper is organized as follows. First, we describe some basic mechanics and test specimens for interface characterization. Examples of measured cohesive laws are given and their effect on

overall interface toughness is discussed. Next, interface cohesive laws are used to predict macroscopic composite cohesive laws, representing crack bridging by cross-over fibres. Effects of interface properties are exploited for both mode I and mixed mode cracking. Finally, composite cohesive laws are used in the prediction of the load -carrying capability of large composite structures.

2. INTERFACE COHESIVE LAWS

In this section experimental methods are described for characterising the mechanical interface properties (fracture energy, cohesive laws, friction laws and fracture resistance curves). Planar, well-defined geometries are used since they allow fundamental studies on surface properties using advanced chemical analysis techniques. Furthermore, the mechanical analysis, by a J integral approach elaborated below, is straightforward.

Interfaces with different properties (weak, intermediate and strong) are created through plasma polymerisation. A thin polymer film (20-150 nm) is deposited on planar substrates. The type and number of chemical functional groups are varied by using different monomers and parameters during plasma polymerisation.

2.1 Test principle. DCB (Double Beam Cantilever) sandwich specimens are loaded by pure bending moments for the measurement of the interface cohesive laws under nominal Mode I (normal opening) as shown in Fig. 3(a). The sandwich specimen consists of two planar substrates bonded together by an adhesive representing the matrix material of a composite, reinforced with steel beams. The J integral (Rice 1968) evaluated along the external boundaries of the specimen gives (Bao et al. 1992)

$$J_{ext} = \frac{1-\nu_2^2}{E_2}\frac{M^2}{B^2H^3\eta^3 I} \ , \tag{1}$$

where E_2 and ν_2 are Young's modulus and Poisson's ratio of the steel. M is the applied moment, H the thickness of the steel beams and B the specimen width. The parameters η and I depend on the geometry and elastic properties of the steel and the substrate (Bao et al. 1992). In (1) the contribution from the adhesive is neglected as its stiffness is much lower than the steel and the substrate. Note from (1) that the J integral is independent of the crack length, a; then for this specimen crack growth is stable.

The J integral along a path just outside the failure process zone is (Rice 1968)

$$J_{ext} = \int_0^{\delta_n^*} \sigma_n^i(\delta_n, \delta_t)\, d\delta_n \ , \tag{2}$$

where δ_n^* is the normal end-opening of the cohesive zone (see Fig. 3(a)) and σ_n^i is the interface cohesive law normal stress. Due to the integration path independence of the J integral, $J_{ext} = J_{loc}$. Differentiation with respect to δ_n^* gives (Suo et al. 1992):

$$\sigma_n^i\left(\delta_n^*\right)=\frac{dJ}{d\delta_n^*}\ , \tag{3}$$

i.e., the cohesive stress as a function of the end-opening (the interface cohesive law under normal openings). Thus, by recording J (via the moment, M) and the end-opening δ_n^* simultaneously during loading until crack growth begins, the interface cohesive law can be obtained from (3).

A precise method is necessary to accurately measure the end-opening of the failure process zone as the deformations are of the order of a micron. Therefore, a Speckle pattern of particles is made on the specimen surface. By following the movement of individual particles across the interface using image analysis the displacements can be determined. A similar approach is to use Digital Image Correlation (Berfield et al. 2007), can also give information about the displacement field near the crack. These measuring techniques can be even used with a normal optical microscope providing sufficient magnification capabilities. In this case sub-pixel resolution techniques usually need to be employed to obtain a sufficient accuracy.

A similar principle can be used to derive the interface cohesive law under pure Mode II. A schematic illustration of a test specimen that could be used for this purpose is shown in Fig. 3(b). The J integral evaluated along the external boundaries can be obtained in closed analytical form. An equation similar to (2) is obtained when evaluating the J integral locally around the failure process zone, except that the interfacial shear appears instead of the normal stress and the tangential end-opening displacement replaces the normal crack opening displacement. This approach enables the determination of the Mode II cohesive law.

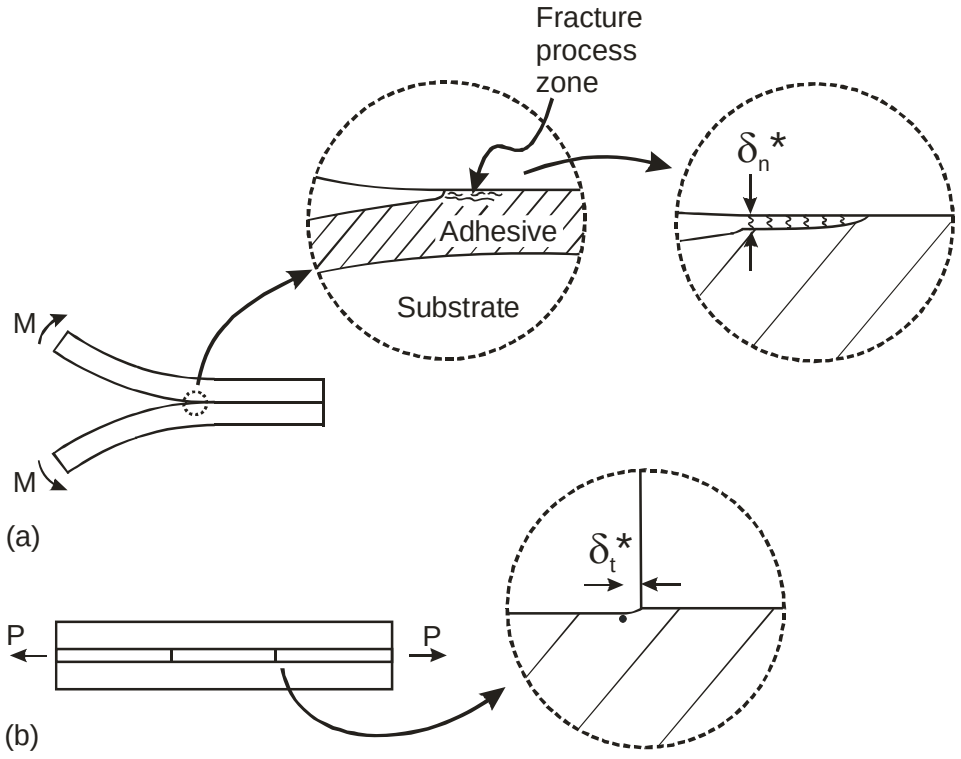

Fig. 3. (a) Schematic illustration of a DCB specimen loaded with pure bending moments for characterising interface properties under Mode I conditions. The adhesive is in between the two substrates. (b) Planar specimen geometry for Mode II interface testing. Two substrates are embedded in an adhesive.

2.2 Example of measurement of interface cohesive law. As an example, planar glassy carbon substrates (Sigradur G, HTW Hochtemperatur, Germany) were used as an experimental model of carbon fibres. Glassy carbon is a fully disordered material in contrast to carbon fibres and its mechanical properties are significantly lower than carbon fibres. However, its chemical properties resemble those of carbon fibres quite well (Launay et al 2007).

Specimens were made as follows. An epoxy resin was poured between two plasma treated glassy carbon substrates (65 x 1 x 5 mm^3). Teflon films, 0.5 mm thick, were used to keep the glassy carbons apart. The cured samples were ground and polished to facilitate optical observations of crack growth. Subsequently the sandwich specimens were reinforced with 6 mm thick stainless steel beams.

During the loading, the end-opening was measured by following the movement of two particles across the interface. Images were recorded using a low magnification optical microscope with a resolution of approximately 650nm per pixel.

Fig. 4 shows a typical result. The J integral is shown as a function of the end-opening. There is realtive large scatter in the measurements of the end-openings. Since the critical crack opening is less than a micron. almost all the details of the cohesive law need to be calculated using sub-pixel calculation for the present the experimental set-up. Thus the interface cohesive law to be derived below should be regarded as an illustrative example of the approach.

Due to uncertainties especially at very low crack openings a linear approximations is used to fit the experimental data. For larger crack openings an exponential function is chosen. The associated interface cohesive law is given in Fig. 5. The ambiguity mainly concerns the shape of the cohesive law and the peak stress; the measured critical crack opening agrees well with openings measured in experiments performed inside the chamber of an ESEM (Environmental Scanning Electron Microscope). For more accurate results a higher magnification microscope or an ESEM should be used.

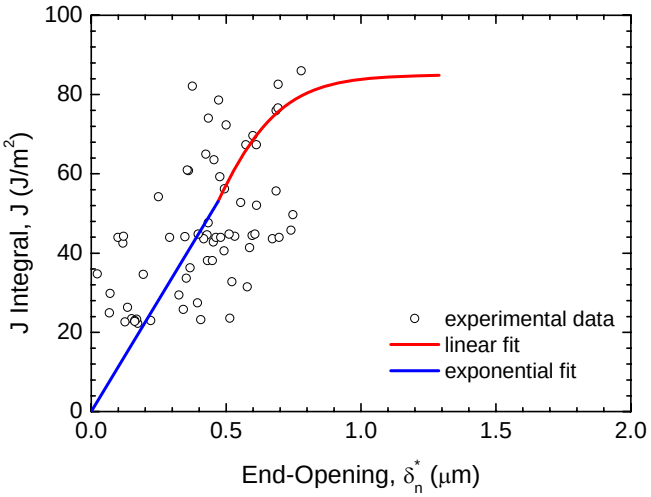

Fig. 4. J integral as a function of the end-opening of the failure process zone.

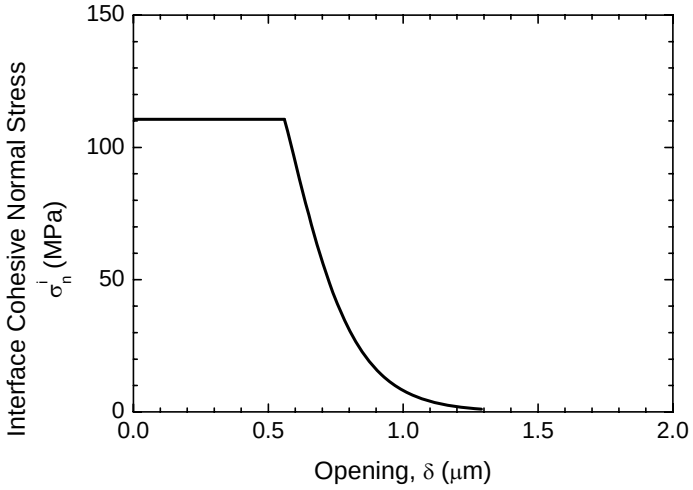

Fig. 5. Interface cohesive law obtained from the data presented in Fig. 4.

2.3 Fracture resistance curves. Once the crack begins to propagate, the fracture resistance, calculated by the J integral no longer represents just the interface cohesive law of fracture process zone; if a plastic zone develops near the crack tip, unloading will take place during crack propagation. As the plastic zone increases in size, the J integral value increases as the crack length increases (R-curve behavior).

Examples of fracture resistance curved are depicted in Fig. 6 for a weak, an intermediate and a strong interface. For the weak interface the fracture energy is almost constant as a function of crack extension. For the intermediate and strong interfaces a significant R-curve behaviour is observed. This extrinsic toughening is probably due to plasticity (Tvergaard and Hutchinson, 1992, 1993). Almost all experiments were terminated by the onset of unstable crack growth with specimens showing R-curve behaviour being more prone to unstable crack growth. In some cases the interface crack kinked into the glassy carbon. The instability characterized by a very high crack velocity and it is possible a visco-plastic effect of the epoxy resin.

3. PREDICTIONS OF COMPOSITE COHESIVE LAWS

3.1 Mechanism of crack bridging by cross-over bridging. Fig. 7 shows a micrograph of the crack bridging mechanism in a unidirectional fibre composite. Single fibres and ligaments consisting of several fibre are attached to the two crack faces and act as a bridge between the two crack faces. The bridging ligaments thus generate tractions that tend to restrain the crack opening. With increasing crack opening, the ligament debonds along an interface, increasing the length of the ligament. Following Bao and Suo (1992) we will call this bridging mechanism for *cross-over bridging*.

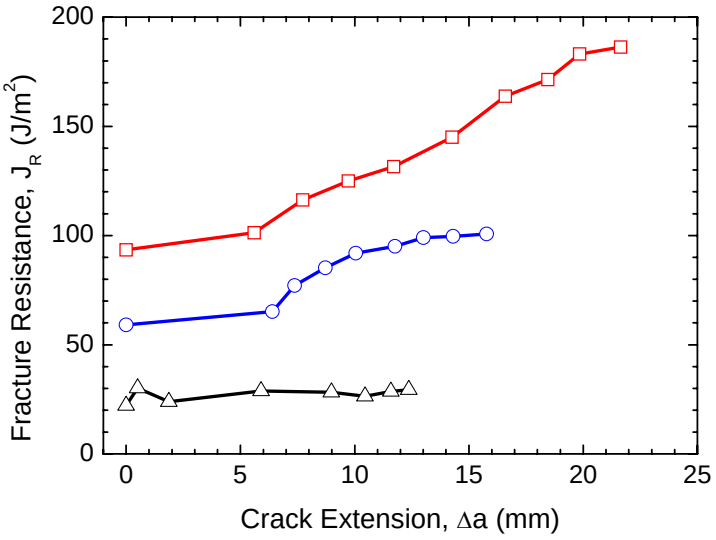

Fig. 6. Fracture resistance curves for a weak (black triangles), intermediate (blue circles) and strong (red squares) interfaces.

3.2 Analytical models for cross-over bridging. An analytical model for Mode I crack bridging by cross-over bridging was developed by Spearing and Evans (1992). They modelled cross-over bridging by a Timoshenko-type beam peeling off along an interface. Their model only describes the interface separation process in one parameter, the interfacial fracture energy, Γ_c^i. Thus, effects of other interface cohesive parameters cannot be uncovered by such a model. Never the less the model gives insightful results. When the shear deformation is neglected, the model predicts a relationship between the normal stress and normal opening at the composite level as (Sørensen and Jacobsen, 1998)

$$\sigma_n^c = \sigma_n^c(\delta_n) = \frac{1}{4}\left[\frac{2}{3}\frac{\Gamma_c^i}{Eh}\right]^{3/4}\sqrt{\frac{2h}{\delta_n}}\,\eta bhE \ , \tag{4}$$

where σ_n^c is the normal stress (superscript c is used for indicate that the equation concerns composite cohesive law), E is the Young's modulus, b and h denote the width and height of the bridging ligaments, η is the number of bridging ligaments per unit crack area and δ_n is the normal opening of the crack. This approximate solution is not expected to be accurate for very short ligaments. Consequently, the singular stress predicted for $\delta_n \to 0$ should not be taken literally.

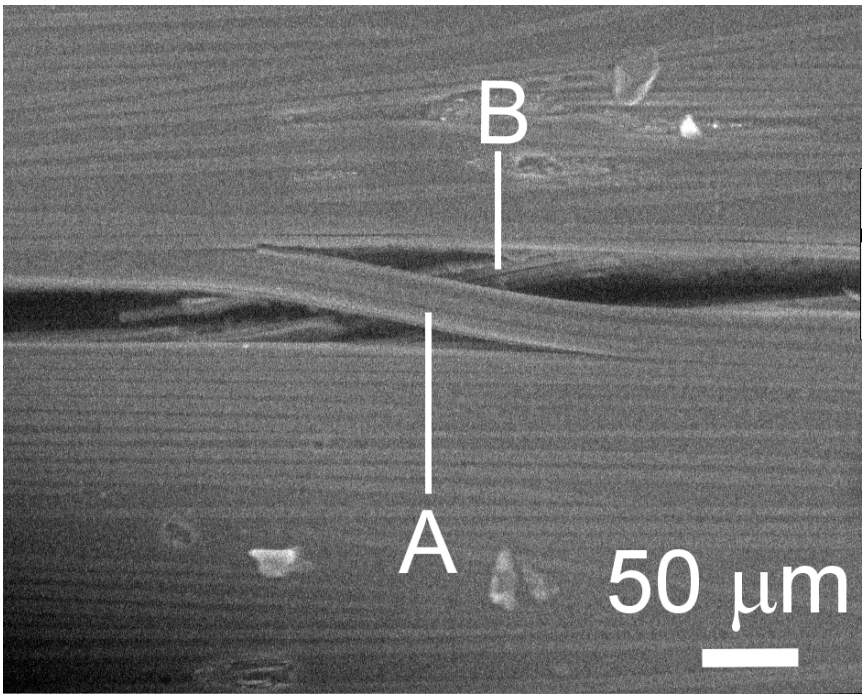

Fig. 7. Micrograph of a cross-over bridging in a unidirectional polymer matrix composite.

Recently, the model of Spearing and Evans was extended to mixed mode (Mode I-II) by Sørensen et al. (2007a). Assuming that only ligaments loaded in axial tension transmit stresses between the crack faces and neglecting shear deformation, the normal stress of the composite cohesive law is predicted to be

$$\frac{\sigma_n^c}{\eta bhE} = \frac{\dfrac{\delta_n}{h}\left[\dfrac{\mathsf{G}_c^i}{Eh}\right]^{3/2}}{\left[\left(\dfrac{\delta_t}{2h}\right)^2 + \sqrt{\left(\dfrac{\delta_t}{2h}\right)^4 + 6\dfrac{\mathsf{G}_c}{Eh}\left(\dfrac{\delta_n}{2h}\right)^2}\right]^{3/2}} \tag{5}$$

where δ_t is the tangential crack opening. The composite cohesive shear stress σ_t^c is found as

$$\frac{\sigma_t^c}{\eta bhE} = \frac{\dfrac{\delta_t}{h}\left[\dfrac{\mathsf{G}_c^i}{Eh}\right]^{1/2}}{\left[\left(\dfrac{\delta_t}{2h}\right)^2 + \sqrt{\left(\dfrac{\delta_t}{2h}\right)^4 + 6\dfrac{\mathsf{G}_c}{Eh}\left(\dfrac{\delta_n}{2h}\right)^2}\right]^{1/2}} \tag{6}$$

A plot of the mixed mode cohesive stresses is shown in Figs. 8 and 9. In the Figures, the cohesive stresses are shown as a function of magnitude of the opening and the phase angle of the end-openings, φ, defined such that $\varphi = 0°$ corresponds to pure normal opening (Mode I) and $\varphi = 90°$ corresponds to pure tangential opening (Mode II).

Fig. 10 shows the predicted fracture resistance curves (the J integral value, J_R, as a function of

the magnitude of the end-opening of the cohesive zone, δ^*) obtained by integration of the bridging stresses locally around the cohesive zone according to the J integral:

$$J_R = \int_0^{\delta_n^*} \sigma_n^c(\delta_n, \delta_t)\, d\delta_n + \int_0^{\delta_t^*} \sigma_t^c(\delta_n, \delta_t)\, d\delta_t \tag{7}$$

where δ_n^* and δ_t^* denote the opening in the normal and tangential directions at the end of the cohesive zone, respectively. It is seen from Fig. 10 that for φ = 0° (Mode I), the fracture resistance increases as $\sqrt{\delta^*}$ in agreement with earlier findings (Sørensen and Jacobsen, 1998). For higher values of φ, the fracture resistance increases almost linearly with δ^*. The model predicts, for the same end opening, a higher fracture resistance for a higher value of φ. Thus, under the assumption of constant η and constant h, the cross-over bridging mechanism is a more effective toughening mechanism under mixed mode and Mode II than under Mode I.

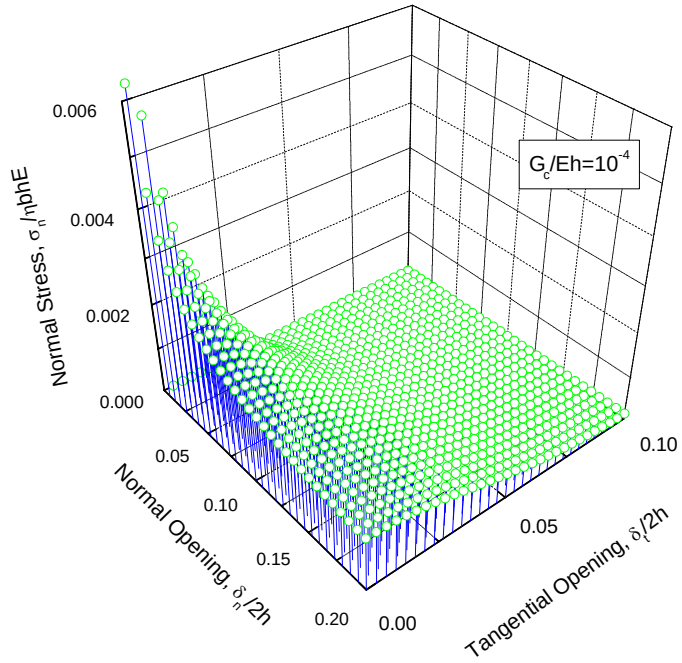

Fig. 8. Normal stress predicted as a function of normal and tangential crack opening displacements.

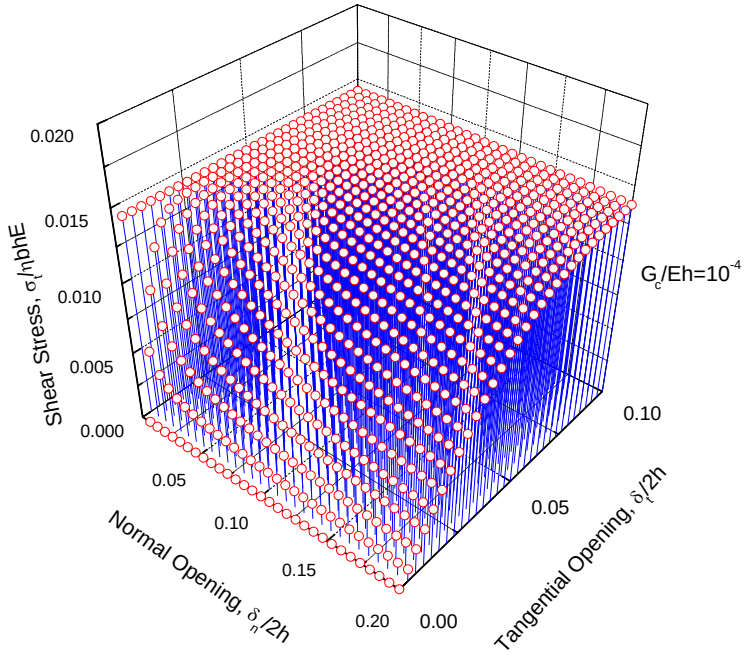

Fig. 9. Composite cohesive law shear stress predicted as a function of normal and tangential crack opening displacements.

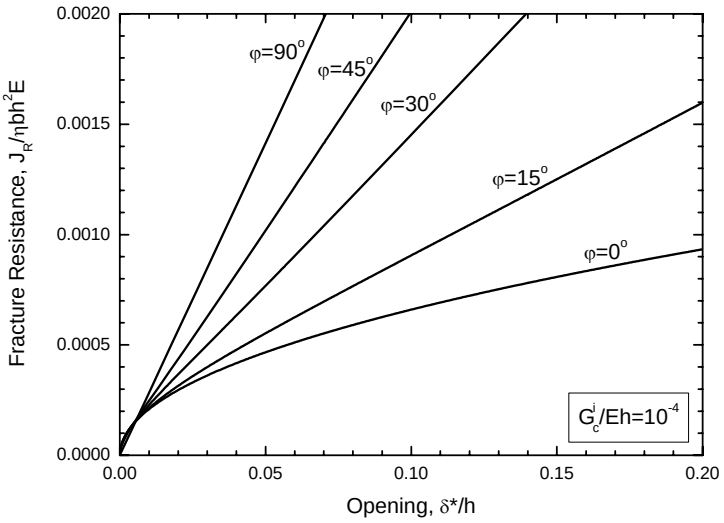

Fig. 10. Fracture resistance curves predicted from the micromechanics model.

3.3 Numerical model for cross-over bridging. Mode I crack bridging was modeled by Østergaaard et al. (2007) using the finite element method that accounts for large displacements and finite strains. The detachment of a bridging ligament along the interface was modeled by the use of a cohesive zone. The interface cohesive law was taken to have the trapezoidal shape proposed by Tvergaard and Hutchinson (1992). Composite cohesive laws were obtained by

prescribing a monotonic opening of the crack faces. The solution was obtained in increments. A stable solution path was obtained by the use of a special Rayleigh-Ritz procedure.

A comparison of a predicted composite cohesive law obtained from the finite element/cohesive zone model and one predicted from the analytical Spearing-Evans model is found in Fig. 11. Here, ℓ is the distance between the bridging ligaments. It is seen from the Figure that the two cohesive laws are in agreement for small crack openings ($\delta_n/h < 2$). For large crack openings the model predictions deviate: The analytical model predicts that the composite cohesive stress decreases asymptotically to zero whereas the numerical results approach a constant value. This difference can be attributed to the fact that the numerical model accounts for finite displacements which the analytical model does not.

The effect of the interface fracture energy, G_c^i, on predicted composite cohesive laws is shown in Fig. 12. A higher interfacial fracture energy results in a higher composite cohesive stress, but the shape is not significantly altered.

Fig. 13 shows the effect of the critical opening for which the interface cohesive stresses vanishes, $\delta_{n,c}^i$ (for at fixed interfacial energy, this is the same as altering the peak interfacial cohesive stress; an increasing is equivalent to a decreasing peak stress). It is seen from the figure that the predicted composite cohesive laws deviate significantly for small openings ($\delta_n/h < 0.5$). A smaller critical opening of the interface cohesive law gives a higher peak stress for the composite cohesive laws. However, for larger openings, the curves converge; the results become insensitive to the critical opening when the ligament length is long.

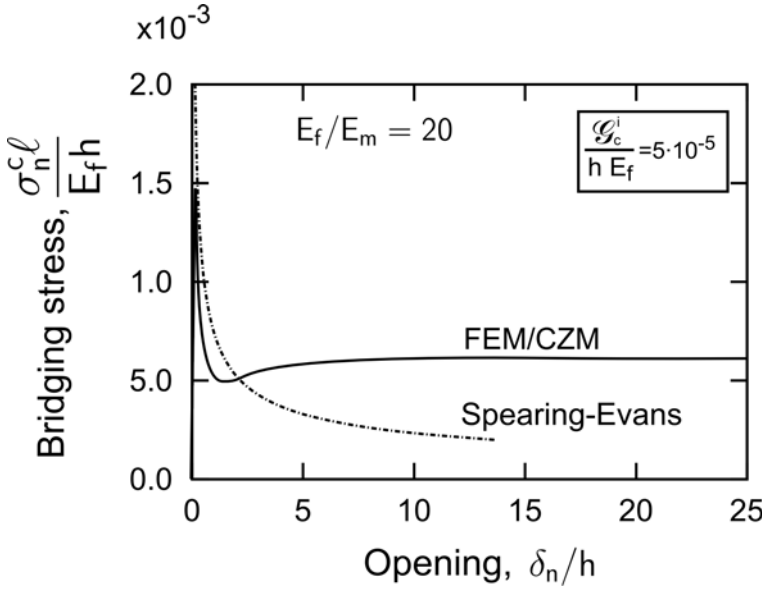

Fig. 11. Comparison of Mode I composite cohesive law predicted by the analytical Spearing-Evans model and predicted by the finite element/cohesive zone model.

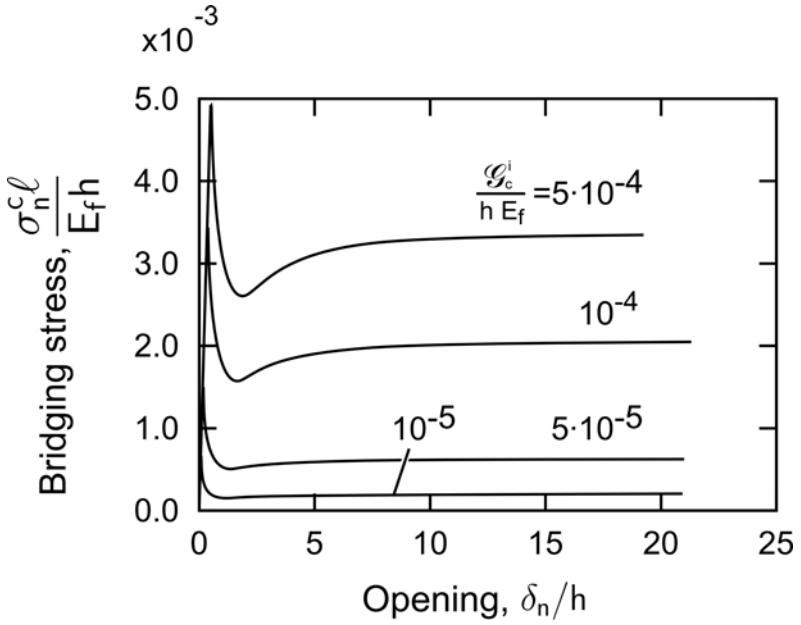

Fig. 12. Effect of interface fracture energy on the Mode I composite cohesive law.

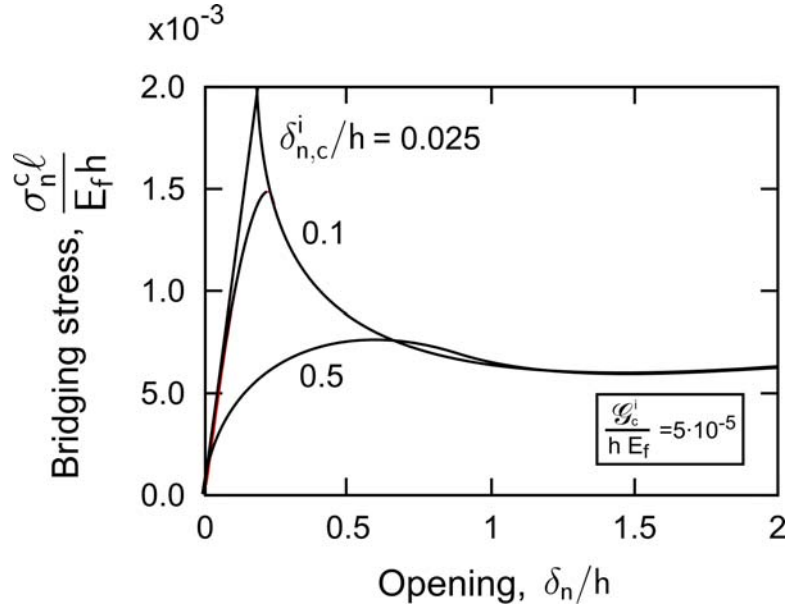

Fig. 13. Effect of the critical separation opening of the interface cohesive law on the Mode I composite cohesive law.

4. MEASUREMENT OF COMPOSITE COHESIVE LAWS

4.1 Approach for the determination of mixed mode cohesive laws. Having made predictions of composite cohesive laws, we proceed to experimental determination of composite cohesive laws. To do so, we utilize a J integral based approach (Sørensen and Kirkegaard 2006). Using the common assumption the composite cohesive law stresses are derived from a potential function, Φ,

$$\sigma_n^c(\delta_n,\delta_t)=\frac{\partial\Phi(\delta_n,\delta_t)}{\partial\delta_n} \qquad \sigma_t^c(\delta_n,\delta_t)=\frac{\partial\Phi(\delta_n,\delta_t)}{\partial\delta_t}, \tag{8}$$

the J integral result (7) becomes

$$J_R = \Phi\left(\delta_n^*, \delta_t^*\right) . \tag{9}$$

Thus, the value of the fracture resistance equals the potential function evaluated at the end openings of the cohesive zone. Combining (8) and (9) gives

$$\sigma_n\left(\delta_n^*, \delta_t^*\right) = \frac{\partial J_R\left(\delta_n^*, \delta_t^*\right)}{\partial \delta_n^*} \qquad \sigma_t\left(\delta_n^*, \delta_t^*\right) = \frac{\partial J_R\left(\delta_n^*, \delta_t^*\right)}{\partial \delta_t^*} \quad . \tag{10}$$

It follows that mixed mode cohesive laws can be derived by simultaneous measurements of J_R, δ_n^* and δ_t^*.

In order to determined fracture resistance in a J integral consistent manner, specimens should be used for which a J integral solution exists also in the case of Large Scale Bridging (LSB). We have used the DCB-specimen loaded with uneven bending moments (DCB-UBM), see Fig. 14. When the distances from the beam ends to the failure process zone are longer than a few times the beam height, the J integral value evaluated along the exterior boundaries of the specimen can be obtained analytically. The result is (plane strain) (Sørensen et al. 2006).

$$J_{ext} = \left(1-\nu^2\right) \frac{21\left(M_1^2 + M_2^2\right) - 6M_1M_2}{4B^2H^3E} \ , \tag{11}$$

where M_1 and M_2 are the applied bending moments (positive signs are shown in the figure), E and ν denotes the Young's modulus and the Poisson's ratio, B is the specimen width and H is the beam height. For plane stress, the factor $1-\nu^2$ should be replaced by unity. J_{ext} equals the fracture resistance, J_R when cracking takes place. Thus, by recording J_R, δ_n^* and δ_t^* during experiments, we can determine the mixed mode cohesive laws from (10).

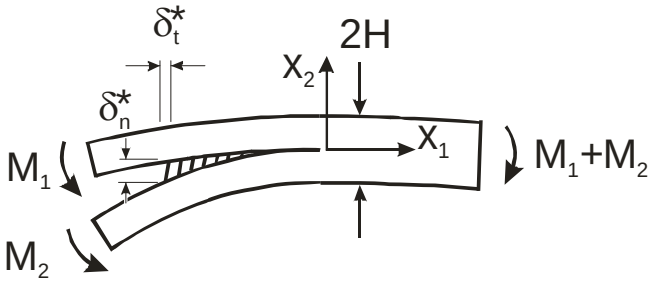

Fig. 14. A fracture mechanics test specimen: The Double Cantilever Beam specimen loaded with Uneven Bending Moments (DCB-UBM).

4.2 Example of measurement. DCB-UBM specimens were made from a plate of a unidirectional glass fibre polymer matrix composite. Fracture mechanics tests were conducted at a special test fixture that applies pure, uneven bending moments to the DCB specimen via two transverse arms, using a wire and roller arrangement (Sørensen et al. 2006). The applied moments as well as displacements at the initial crack tip (that becomes the end-opening of the cohesive zone) were recorded during the tests. After the tests, J_R was calculated using (11) and a fit (orthogonal

polynomials) was made to the J_R-δ_n^*-δ_t^* data. The cohesive laws were then obtained by partial differentiation according to (10). Here, only the pertinent results will be reviewed; details about the specimen manufacture, testing approach and data analysis are given elsewhere (Sørensen and Jacobsen 2007).

Fracture resistance curves, J_R as a function of δ^* are shown in Fig. 15 for various ratios of the applied moments. Here, M_1/M_2 = -1 corresponds to Mode I and M_1/M_2 = 1 corresponds to Mode II. Fig. 16 shows the recorded δ_n^*-δ_t^* data. It is seen from Fig. 16 that $M_1/M_2 < 0$ results in end-openings dominated by normal opening, δ_n^*. Only for M_1/M_2 approaching 1 the openings becomes dominated by δ_t^*. Observe from Fig. 15 that the fracture resistance curves of the δ_n^*-dominated experiments are smooth, indicating completely stable crack growth; the fracture resistance curves has a rough form due to rapid decrease in load with increasing amount of δ_t^*. Furthermore, and the curves do not flatten out to attain steady-state values with increasing amount of δ_t^*; rather they take a nearly constant slope. Comparing the experimental fracture resistance data with the prediction of the mixed mode micromechanics model (Fig. 10) we observe that they are qualitatively similar in form.

Composite cohesive laws obtained from the fracture resistance data are shown in Fig. 17 and Fig. 18. Only data until the transition to steady-state are plotted. Fig. 17 shows the cohesive normal stress, σ_n^c, as a function of δ_n and δ_t. We find that σ_n^c has a peak value $\hat{\sigma}_n^c \approx 8$ MPa near (δ_n, δ_t) = (0, 0), but decreases rapidly with increasing values of δ_n and δ_t. In the region near pure Mode II ($\delta_n^* \approx 0$ - 0.5 mm), σ_n^c comes out being negative (i.e., compressive) around $\delta_t \approx 0.3$ - 0.7 mm; the minimum value is about -1.7 MPa. For $\delta_t \approx 1$ - 2 mm, σ_n^c increases to a near-constant value around 1-2 MPa.

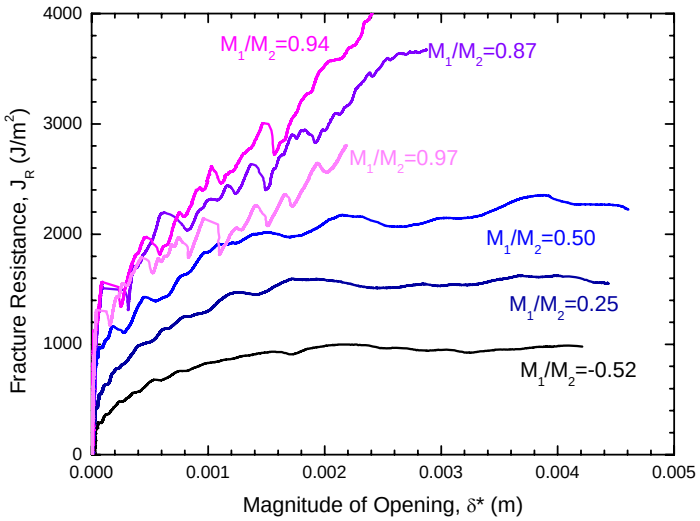

Fig. 15. Measured fracture resistance data for various M_1/M_2 ratios.

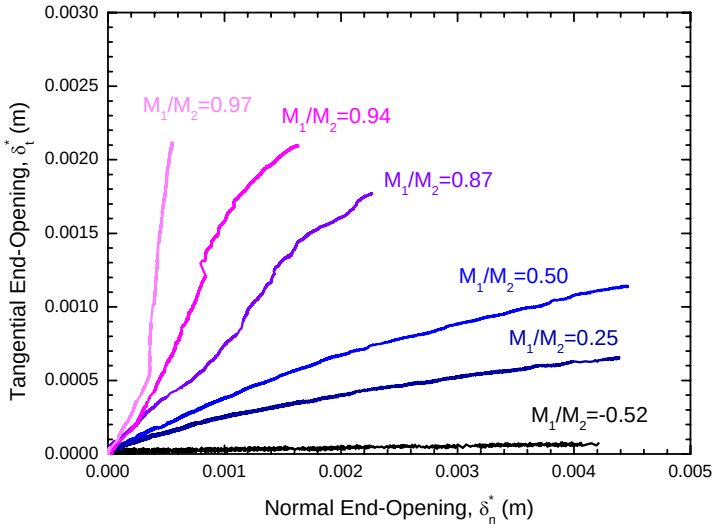

Fig. 16. Measured end-openings for various M_1/M_2 ratios.

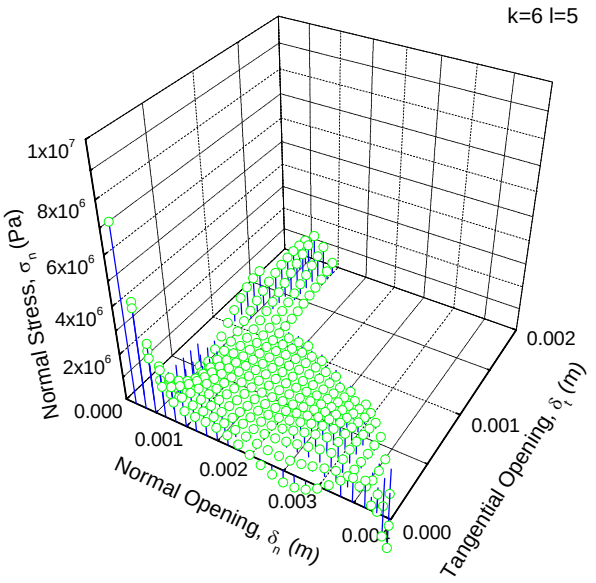

Fig. 17. Composite cohesive laws obtained from the mixed mode fracture mechanics data: The normal stress as a function of the normal and tangential crack opening displacements.

The cohesive shear stress, σ_t^c, is shown in Fig. 18. The peak value, $\hat{\sigma}_t^c$, around 15-22 MPa, is found to be located at (δ_n, δ_t) = (0, 0). Away from the origin, σ_t^c decreases to a near constant value of 1-2 MPa. For $\delta_n \approx 0$, σ_t varies in a wavy fashion around zero, in particularly at $\delta_n \approx 4$ mm. This wavy behaviour is considered invalid, since σ_t is expected to vanish for $\delta_n = 0$.

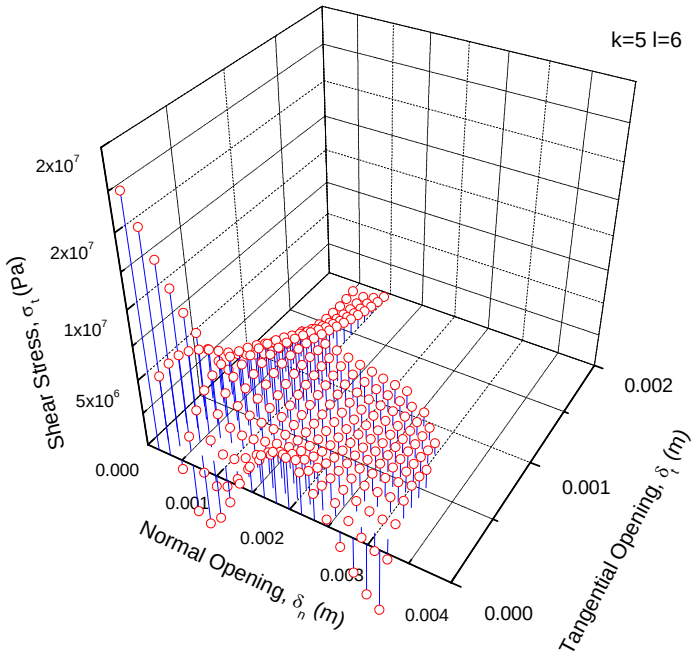

Fig. 18. Composite cohesive laws obtained from the mixed mode fracture mechanics data: The shear stress as a function of the normal and tangential crack opening displacements.

5. PREDICTION OF RESPONSE OF STRUCTURES FROM COMPOSITE COHESIVE LAWS

5.1 Outline for a case story: Medium scale adhesive joint specimens. We now proceed to use composite cohesive laws for the prediction of structural behavior of a large structure. The problem that we consider is crack growth along the interface of an adhesive joint joining two parts made of unidirectional polymer matrix composite consisting on nearly unidirectional glass fibres. The specimens are 2 meter in length; we will refer to them as "medium" size specimens, since they are significantly larger than standard laboratory specimens, but smaller than real structural parts like a wind turbine blade. The medium size specimen is loaded in four-point flexure, as shown schematically in Fig. 19. Three ratios of the thickness of the two parts (denoted h_1 and h_2, respectively) were investigated. The cracking problem involves LSB due to cross-over bridging; this invalidates the use of LEFM. Instead, composite cohesive laws will be used in the strength prediction.

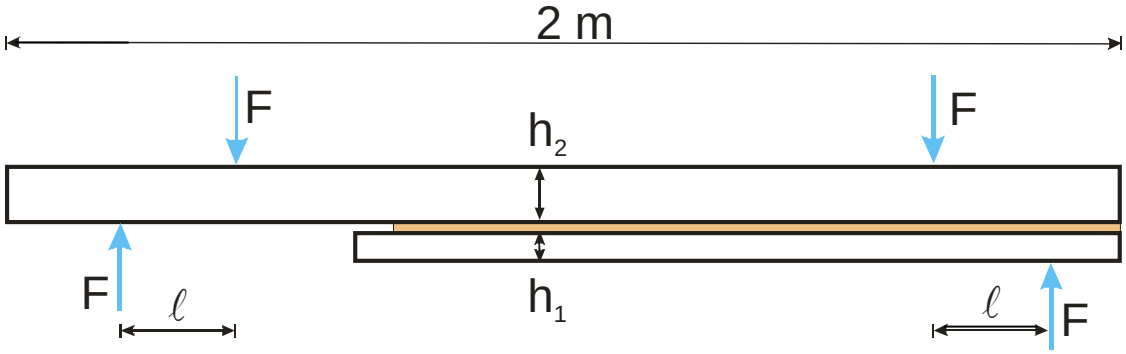

Fig. 19. Geometry and loading of medium scale specimens.

We continue as follows. First, fracture mechanics testing (using the DCB-UBM specimen shown in Fig. 14) was used for measurement of the fracture resistance of the adhesive joint under the full combination of loads, from M_1/M_2 = -1 to M_1/M_2 = 1. The steady-state fracture resistance was 2.0 kJ/m^2 for Mode I and 4.0 kJ/m^2 for Mode II. Furthermore, the normal and tangential crack opening displacement where the cohesive stresses vanish under pure Mode I and pure Mode II, denoted $\delta_{n,0}^c$ and $\delta_{n,0}^c$ respectively, were determined to be $\delta_{n,0}^c$ = 1.8 mm and $\delta_{t,0}^c$ = 0.2 mm. Having established the fracture resistance data, parameters for composite cohesive laws were determined.

Independent linear softening composite cohesive laws were used for the normal and shear stresses

$$\sigma_n^c = \hat{\sigma}_n^c \left(1 - \frac{\delta_n}{\delta_{n,0}^c}\right) \qquad \sigma_t^c = \hat{\sigma}_t^c \left(1 - \frac{\delta_t}{\delta_{t,0}^c}\right). \tag{12}$$

Noting from (7) that the area under the cohesive laws equals the steady-state fracture resistance, the following values were obtained for the peak stresses: $\hat{\sigma}_n^c$ = 2.2 MPa and $\hat{\sigma}_t^c$ = 40 MPa.

Second, the problem was modeled with the aim of simulation the crack growth and thereby predicting the load-carrying capacity. The cracking was modeled by cohesive zone modeling using the commercial code Abaqus (version 6.6). The explicit version was used to solve the problem under quasi-static conditions (the kinetic energy of the model was a small fraction of the total energy). The increment in moment was prescribed by controlling the rotation of the beam in using a procedure developed by Jacobsen and Sørensen (2001). A quadratic traction-interaction failure criterion was used for damage initiation in the cohesive elements under mixed mode conditions

$$\left(\frac{\sigma_n^c}{\hat{\sigma}_n^c}\right)^2 + \left(\frac{\sigma_t^c}{\hat{\sigma}_t^c}\right)^2 = 1. \tag{13}$$

Third, 2 meter long medium size specimens were manufactured and tested under four-point flexure. The medium size specimens were tested under four-point flexure. Data for the applied moment and the crack length were recorded during the cracking of the specimens. More details about the experiments and modelling will be published elsewhere (Sørensen et al. 2007b).

5.2 Experimental and model results. Results, in the form of the applied moment at crack growth as a function of crack extension are shown in Fig. 20. Both experimental results and mode predictions are shown. It is seen that there is a good agreement with the overall trend of the experiments and predictions: the fracture resistance rises and attains a (steady-state) value. Both experiments and simulations show that the moment at steady-state cracking was highest for the specimens having the smallest h_1.

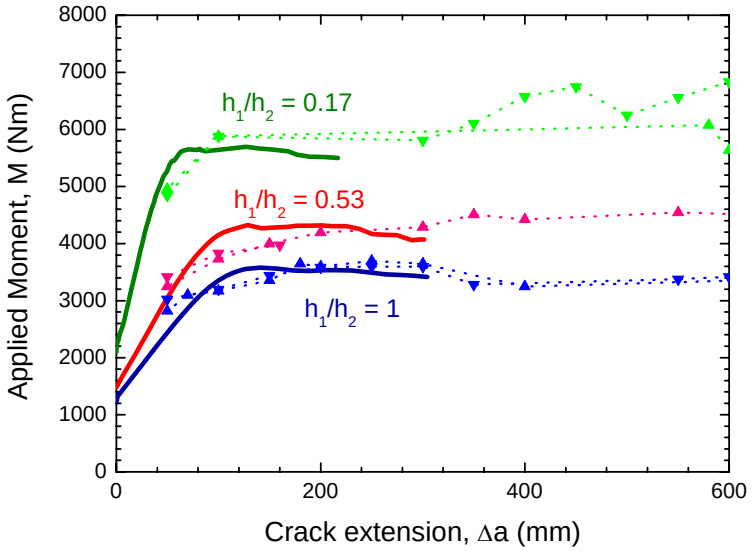

Fig. 20. Predicted and measured relationship between crack length and the applied moment. Dotted lines with symbols are experimental data; solid curves are mode predictions.

6. SUMMARY AND CONCLUSIONS

Experiments and modeling has been performed for the study of the connection between interface properties and overall macroscopic strength properties. Experimental methods for the determination of interface cohesive laws have been established. Models have been developed for predicting composite cohesive laws from interface cohesive laws. Strength prediction from composite cohesive laws was demonstrated.

ACKNOWLEDGEMENTS

This research was supported by the STVF Frame Work Programme "Interface Design of Composite Materials", Grant no. 26-03-0160.

REFERENCES

Bao, G. and Suo, Z. (1992). Remarks on crack-bridging concepts", Applied Mech. Rev. 45, 355-61.

Bao, G., Ho, S., Suo, Z., and Fan, B. (1992). The role of material orthopy in fracture specimens for composites", Int. J. Solids Structures 29, 1105-16.

Berfield, T.A., Patel, J.K, Shimmin, R.G., Braun, P.V., Lambros, J. and Sottos, N.R. (2007). Micro- and nanoscale deformation measurement of surface and internal planes via digital image correlation. Exp. Mech. 47, 51-62.

Brøndsted, P., Lilholt, H., and Lystrup, Aa. (2005). Composite materials for wind power turbine blades", Annu. Rev. Mater. Res. 35, 505-38.

Jacobsen, T. K., and Sørensen, B. F. (2001). Mode I Intra-laminar crack growth in composites - modelling of R-curves from measured bridging laws. Composites part A 32, 1-11.

Mohammad, I., and Liechti, K. M. (2000). Cohesive zone modelling of crack nucleation at bimaterial corner", Journal of the Mechanics and Physics of Solids. 48, 735-64.

Launay, H ., Hansen, C. M., and Almdal, K. (2007). Carbon, submitted.

Needleman, A. (1987). A continuum model for void nucleation by inclusion debonding", J. Appl. Mechn. 54, 525-531.

Rice, J. R. (1968). A path independent integral and the approximate analysis of strain concentrations by notches and cracks. J. Appl. Mech. 35, 379-86.

Suo, Z., Bao, G., and Fan, B. (1992). Delamination R-curve phenomena due to damage. J. Mech. Phys. Solids. 40, 1-16.

Spearing, S. M., and Evans, A. G. (1992). The role of fiber bridging in the delamination resistance of fiber-reinforced composites. Acta Metall. Mater. 40, 2191-9.

Sørensen, B. F., Gamstedt, E. K., Østergaard, R. C., and Goutianos, S. (2007a). Micromechanical model of cross-over fibre bridging - prediction of mixed mode bridging laws. Mechanics of Materials, accepted.

Sørensen, B. F., Goutianos, S., and Jacobsen, T. K. (2007b). Strength scaling mechanics of polymer composites. Composites part A, manuscript in progress.

Sørensen, B. F. and Jacobsen, T. K. (1998). Large scale bridging in composites: R-curve and bridging laws. Composites part A 29, 1443-51.

Sørensen, B. F., and Jacobsen, T. K. (2007). Characterizing delamination of fibre composites by mixed mode cohesive laws. Journal of the Mechanics and Physics of Solids, submitted.

Sørensen, B. F., Jørgensen, K., Jacobsen, T. K., and Østergaard, R. C. (2006). DCB-specimen loaded with uneven bending moments. International Journal of Fracture 141, 159-172.

Sørensen, B. F., and Kirkegaard, P. (2006). Determination of mixed mode cohesive laws. Engineering Fracture Mechanics 73, 2642-61.

Tvergaard, V., and Hutchinson, J. W. (1992). The relation between crack growth resistance and fracture process parameters in elastic-plastic solids. J. Mech. Phys. Solids 40. 1377-97.

Tvergaard, V., and Hutchinson, J. W. (1993). The influence of plasticity on mixed mode interface toughness. Journal of the Mechanics and Physics of Solids 41, 1119-35.

Webb, T. E., and Aifantis, E. C. (1995). Oscillatory fracture in polymer materials. Int. J. Solids Structures 32, 2725-43.

Yang, Q, and Cox, B. (2005). Cohesive models for damage evolution in laminated composites. Int. J. Fract. 133, 107-37.

Yang, Q. D. and Thouless, M. D. (2001). Mixed-mode fracture analysis of plastically-deforming adhesive joints. Int. J. Fracture. 110, 175-87.

Østergaard, R. C. and Sørensen B.F. (2007), Prediction of composite scale cohesive law for delamination with fiber bridging, to appear.